Geophysical Prospecting EAGE EUROPEAN ASSOCIATION OF GEOSCIENTISTS & ENGINEERS

Geophysical Prospecting, 2012, **60**, 838–854 doi: 10.1111/j.1365-2478.2011.01020.x

Virtual signals combination – phase analysis for 2D and 3D data representation (acoustic medium)

Flavio Poletto[1]*, Cinzia Bellezza[1], Kees Wapenaar[2] and Aronne Craglietto[1]

[1]*OGS – Istituto Nazionale di Oceanografia e di Geofisica Sperimentale Borgo Grotta Gigante 42/c, 34010 Sgonico (Trieste), Italy, and*
[2]*Department of Geoscience and Engineering, Delft University of Technology PO Box 5048, 2600 GA Delft, The Netherlands*

Received November 2010, revision accepted August 2011

ABSTRACT

We formulate the Kirchhoff-Helmholtz representation theory for the combination of seismic interferometry signals synthesized by cross-correlation and by cross-convolution in acoustic media. The approach estimates the phase of the virtual reflections from the boundary encompassing a volume of interest and subtracts these virtual reflections from the total seismic-interferometry wavefield. The reliability of the combination result, relevant for seismic exploration, depends on the stationary-phase and local completeness in partial coverage regions. The analysis shows the differences in the phase of the corresponding seismic interferometry (by cross-correlation) and virtual reflector (by cross-convolution) signals obtained by 2D and 3D formulations, with synthetic examples performed to remove water layer multiples in ocean bottom seismic (OBS) acoustic data.

Key words: Passive method, Seismics, Acoustics, Theory.

INTRODUCTION

In recent years virtual seismic methods have been introduced to synthesize new seismic signals by processing traces from a plurality of sources and receivers. These methods need only field measurements and do not need to know the subsurface velocity model. The commonly used seismic interferometry by cross-correlation approach makes it possible to reconstruct the Green's function of the total wavefield between receivers when receivers are completely surrounded by sources (e.g., Snieder 2004; Bakulin and Calvert 2006; Wapenaar and Fokkema 2006; Wapenaar, Draganov and Robertsson 2008; Schuster 2009). The interferometry method is also used by cross-convolution to extrapolate the wavefield in open configurations with one receiver outside the domain (Slob and Wapenaar 2007; Halliday *et al.* 2010). The virtual reflector method based on integral cross-convolution (Poletto and Farina 2008; Poletto and Wapenaar 2009) makes it possible to reconstruct the signal of a virtual reflector at receivers (sources) with sources (receivers) included in the volume of interest. The virtual reflector method needs impulsive or transient and known sources.

An advantage of utilizing interferometry by cross-correlation and by cross-convolution is that they can be used to reconstruct the same reflection events for a data set recorded (or emitted) at a boundary. This makes it possible to remove boundary-related reflections present in both these virtual signals. Examples of water-layer multiple attenuation using the virtual signals of synthetic ocean bottom seismic (OBS) data with sources in the proximity of the sea-surface are discussed by Poletto and Farina (2010b). The main goal of this paper is to determine the phase relations between these virtual results in 2D and 3D. We analyse the combination of the interferometry-by-correlation and virtual reflector methods (Poletto and Farina 2008, 2010a,b; Poletto, Wapenaar and Bellezza 2010), formulating the Kirchhoff-Helmholtz integral

*E-mail: fpoletto@ogs.trieste.it

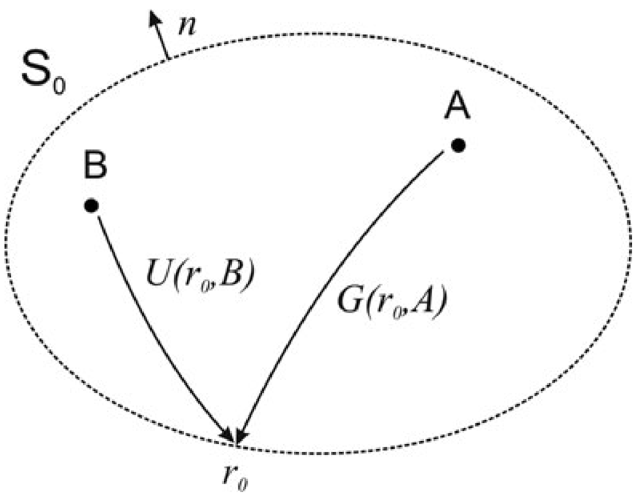

Figure 1 Kirchhoff-Helmholtz representation concept. U and G represent the propagating wavefield and the Green's function, respectively. The wavefields in the volume encompassed by the surface S_O are represented by integrating the crosscomposition of the wavefields produced by the sources in A and B and measured on S_O.

representation of virtual signal combination in acoustic media (Wapenaar and Fokkema 2006; Poletto and Wapenaar 2009). The approach uses the same source/receiver geometries for seismic interferometry and for the virtual reflector method. Without loss of generality, we introduce the representation models with sources surrounded by receivers (Fig. 1). It is intended that, invoking reciprocity, this is equivalent of using receivers surrounded by sources, so that the results of this analysis also hold when we interchange sources and receivers.

The analysis shows that the estimate of the reflection wavefields by the virtual reflector method can be used to subtract the reflections generated at the representation boundary from the interferometry total wavefield, thus providing an estimate of the Green's function between points buried in a propagation volume without reflections from the encompassing boundary. This task is substantially achieved by cross-convolving the Green's function G, subject to boundary conditions at the representation surface with a combination of the propagating wavefield U and its time reversal expressed by U^* in the Fourier frequency domain, where '$*$' denotes the complex conjugate. We observe that this approach can be seen in a wider context than only for interferometry. For example, it is similar to calculating simultaneous forward and backward propagation of water-layer seismic multiples for the attenuation of water-bottom multiples by wave-equation-based prediction and subtraction (Wiggins 1988, 1999). The approach is also similar to the approach proposed by Wapenaar (1993) to describe forward and backward Kirchhoff-Helmholtz extrapolation of downgoing and upgoing seismic waves in a layered medium with curved interfaces, using model-based Green's functions. The method has applications in acoustics and seismic exploration and may have other applications with electromagnetic signals, etc.

The virtual-signal combination approach presented in this paper does not require the propagation model. We show that it can be useful for interferometry as well as when we select events in one of the terms and that, in general, it can be used as an approximation with the total wavefields for interferometry representations.

THEORY

Virtual reflector representation

We formulate the representation for virtual wavefields propagating in an arbitrary, inhomogeneous, acoustic medium. We assume appropriate recording conditions for virtual signal reconstruction, with complete and partial distributions of receivers around sources (or sources around receivers). For simplicity, we assume unit source signals $S(\omega)$ in the Fourier frequency domain, where ω is the angular frequency, so that we can approximate

$$S(\omega)S^*(\omega) \cong S(\omega)S(\omega) \cong 1, \tag{1}$$

i.e., we can neglect the source signature in the analysis of cross-correlations and cross-convolutions (Poletto and Farina 2010b). The virtual reflector (VR) signal between two points A and B enclosed in a volume encompassed by a surface S_o can be expressed in the Fourier frequency domain by the Kirchhoff-Helmholtz integral representation (Poletto and Wapenaar 2009)

$$U(A, B, \omega) - G(B, A, \omega) = \frac{1}{4\pi}\int_{S_o} dS_o \left[G(r_o, A, \omega)\,\frac{\partial U(r_o, B, \omega)}{\partial n} - U(r_o, B, \omega)\,\frac{\partial G(r_o, A, \omega)}{\partial n} \right], \tag{2}$$

where $U(r_o, B, \omega)$ is the scalar field from a source at point B recorded along the 'reflection' surface S_o, r_o is location along the surface, $G(r_o, A, \omega)$ is the Green's function from an arbitrary source point A to r_o and, $\partial/\partial n$ is the normal differentiation operator acting on r_o at surface S_o (Fig. 1). The scalar functions U and G are Fourier frequency transforms of causal functions. In equation (2), U and G can have, in turn, equivalent propagation- and transfer-function meanings but for different boundary conditions at surface S_o. Note that here we use different symbols to represent U and G, instead of U alone, to better distinguish between the contributions related to the different boundary conditions. Assume that the required boundary condition for G on S_o is rigid with

$$\frac{\partial G}{\partial n} = 0 \tag{3}$$

(*Neumann* boundary condition, with reflection coefficient $R = +1$). No reflecting boundary condition is set on S_o for the free-space solution U. From equation (2) we have

$$U(A, B, \omega) - G(B, A, \omega) = \frac{1}{4\pi} \int_{S_o} dS_o G(r_o, A, \omega) \frac{\partial U(r_o, B, \omega)}{\partial n}, \tag{4}$$

which can be approximated by

$$U(A, B, \omega) - G(B, A, \omega) = \frac{-i\omega}{4\pi c} \int_{S_o} dS_o G(r_o, A, \omega)\ U(r_o, B, \omega) \cos\gamma, \tag{5}$$

where γ is the angle between the ray $U(r_o, B, \omega)$ with respect to the normal to S_o in r_o and where we have used the far-field normal-derivative approximation $\partial/\partial n \cong -i\omega \cos\gamma/c$ at S_o, where c is the acoustic velocity and $i = \sqrt{-1}$. The function

$$V_R(A, B, \omega) = U(A, B, \omega) - G(B, A, \omega) \tag{6}$$

is defined (Poletto and Wapenaar 2009) as the virtual-reflector signal obtained by convolutional equation (5). By construction, V_R is the Fourier frequency transform of a causal function. It contains only reflections, from the surface S_o, of the unit-source signal propagated from the origin point B of function U and received in origin point A of the wavefield G, or vice versa by reciprocity. No direct arrivals between these source points are simulated by equation (6).

To interpret the wavefields of equation (6), we simplify the notation by neglecting – where not required – the explicit dependence on ω in the scalar functions. Function G contains the direct wave and the reflected (from S_o) wavefield (Fig. 2). For a 'ghost-model' reflection (see the next example) we have

$$G(B, A) = G_D(B, A) + G_R(B, A). \tag{7}$$

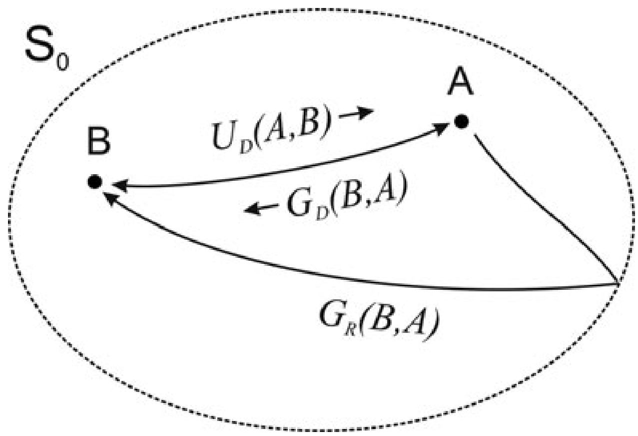

Figure 2 Direct and reflected waves from source B of the propagated wavefield U to the source of the Green's function G, enclosed by the surrounding surface S_o where the waves are measured.

Note that the reflection G_R, represented in Fig. 2 by only one raypath for simplicity, may also contain complex multiple arrivals. The free-space function U contains only the direct wave (since no reflecting boundary conditions are set for U on S_o, however it may contain reflections if we assume non-uniform media) and we have in equation (6)

$$U(A, B) = U_D(A, B). \tag{8}$$

Assuming the equivalence condition for the direct wavefields of the propagating and of the Green's functions, we have

$$G_D(A, B) = U_D(B, A). \tag{9}$$

Moreover, using reciprocity for the representation of the scalar function G gives

$$G_R(A, B) = G_R(B, A) \tag{10}$$

and we obtain from equations (5) and (6) the virtual reflector signal as the opposite of the ghost reflection (as in the initial virtual reflector definition given, apart from with a scalar factor the sign is not relevant)

$$V_R(A, B) = -G_R(A, B). \tag{11}$$

The virtual reflector representation of the boundary reflection in terms of the wavefields measured on S_o becomes

$$G_R(A, B, \omega) \cong \frac{i\omega}{4\pi c} \int_{S_o} dS_o\ G(r_o, A, \omega)\ U(r_o, B, \omega) \cos\gamma. \tag{12}$$

Interferometry representation

To obtain the cross-correlation virtual signal corresponding to the cross-convolution result of equation (12), we use interferometry by cross-correlation with complete coverage in the reciprocal sense, i.e., with source/receiver geometry interchanged with respect to the conventional one. The two sources in A and B are surrounded by receivers located on the enclosing surface S_o, as in Fig. 1 where we have a complete coverage (say complete observation) condition. In other words, integration is performed on the receiver space. This gives the unusual result of synthesizing a virtual seismic receiver at a source position (Curtis *et al.* 2009; Poletto and Farina 2010a). We assume unit sources of volume injection at the points A and B (equation (1)).

We obtain the estimate of the wavefields by using the acoustic reciprocity theorem of correlation type. To obtain this formulation, we modify equation (18) of Wapenaar and Fokkema (2006) for a lossless, constant density medium by using the modified Green's function $G = (1/i\omega\rho)\hat{G}$, where ρ is the medium density, which gives

$$U(A, B) - G^*(B, A) = \frac{1}{4\pi}\int_{S_o} dS_o \left[G^*(r_o, A)\frac{\partial U(r_o, B)}{\partial n} - U(r_o, B)\frac{\partial G^*(r_o, A)}{\partial n}\right], \tag{13}$$

where '$*$' denotes the complex conjugate. Note that in the present form, U and G in equation (13) may again obey different boundary conditions at S_o, similar as in equation (2). Equation (13) is similar to equation (2), with the relevant difference that while the result of equation (2) is the Fourier frequency transform of a causal signal, the result of equation (13) is the sum of the Fourier frequency transforms of one causal and one anticausal signal. For convenience, we take the complex conjugate of equation (13), which becomes

$$U^*(A, B) - G(B, A) = \frac{1}{4\pi}\int_{S_o} dS_o \left[G(r_o, A)\frac{\partial U^*(r_o, B)}{\partial n} - U^*(r_o, B)\frac{\partial G(r_o, A)}{\partial n}\right]. \tag{14}$$

Using the reflecting boundary condition expressed by equation (3) for G on S_o, we obtain

$$U^*(A, B) - G(B, A) = \frac{1}{4\pi}\int_{S_o} dS_o G(r_o, A)\frac{\partial U^*(r_o, B)}{\partial n}, \tag{15}$$

and we can approximate

$$G(B, A, \omega) - U^*(A, B, \omega) = \frac{-i\omega}{4\pi c}\int_{S_o} dS_o G(r_o, A, \omega)\, U^*(r_o, B, \omega)\cos\gamma. \tag{16}$$

Virtual signals combination

In this section we discuss the combinations of the interferometry and virtual reflector wavefields expressed by equations (16) and (12). In the conventional seismic interferometry representation both the crosscorrelated functions are measured wavefields, while in the virtual reflector synthesis one crossconvolved term is the free-space solution. Moreover, the seismic exploration interferometry signals are usually illuminated only by surface sources (except for the situation of passive sources, e.g., Draganov, Wapenaar and Thorbecke 2006), so that the illumination of the free-boundary from below is poor, except in special cases, like with marine multiples. The joint use of these virtual results poses the problem to properly define their boundary conditions, which are intended to be different in separate applications for the virtual reflector method and interferometry. Different approaches can be adopted to perform the combination process. The first one is to use the measured wavefield on S_o in place of the free boundary solution term as an approximation for the virtual reflector representation (Poletto and Wapenaar 2009). This approach may cause distortions in the higher order virtual reflections (Poletto and Farina 2010b). The second approach consists in selecting only the direct wavefield in one of the cross-composed terms for both the integral representations. We may observe that this approach is commonly used to mitigate spurious arrivals in seismic interferometry. This result is achieved by time-gating the traces to preserve only the energy of the direct arrivals in one of the cross-correlated terms (e.g., Bakulin and Calvert 2006).

The combination of the virtual reflector and interferometry equations allows us to subtract the reflected wavefield from the interferometry signal (Poletto and Farina 2010a), provided that they are obtained with similar source-receiver geometry. With complete coverage, the seismic interferometry signal contains the total wavefield, composed of the direct and reflected wavefields. Using equation (7) and subtracting equation (12) from (16) gives

$$G_D(A, B, \omega) - U^*(A, B, \omega) \cong \frac{-i\omega}{4\pi c}\int_{S_o} dS_o G(r_o, A, \omega) \left[U^*(r_o, B, \omega) + U(r_o, B, \omega)\right]\cos\gamma, \tag{17}$$

which is equivalent to calculating the combination of the cross-correlation and cross-convolution integrals as proposed by Poletto and Farina (2008). In other words, we obtain an estimate of the direct wavefield $G_D(A, B, t)$ between B and A without reflections from S_o by inverse Fourier transforming equation (17) and taking the causal part. Equation (17) is obtained for the rigid (Neumann) boundary condition at S_o. The approach can be generalized for arbitrary reflection conditions. More in general, the combination of the virtual signals can be expressed by cross-composing the signals measured on S_o in the form (Poletto and Farina 2008)

$$C(A, B, \omega) = \frac{-i\omega}{4\pi c}\int_{S_o} dS_o G(r_o, A, \omega) \left[\alpha\ U^*(r_o, B, \omega) + \beta\ U(r_o, B, \omega)\right], \quad (18)$$

where the combination weights α and β can be functions of ω to compensate for non-ideal source properties and may depend also on r_o when information on the reflector properties are available for the representation of the scattered wavefields (Poletto and Wapenaar 2009). The joint application by equation (18) exploits its utility when corresponding reflection events are reconstructed both by the virtual reflector and by the interferometry methods. We have previously discussed basic aspects related to the limitations and to the approximations of the approach: essentially for the different boundary conditions on the representation surface and for the different coverage usable to reconstruct the reflected wavefields. Relevant examples may be found as related to acoustic applications, e.g., to determine and separate the reflections in a cavity. Other examples find their utility in the framework of exploration seismics. In this context, the presence of reflections like multiples, e.g., water layer multiples, may contribute to increase coverage and play a key role in the wavefield representation for virtual signal combination purposes. This is relevant since the estimation, processing and separation of multiple reflections is one of the key targets in seismic exploration applications.

In this work we assume that the above mentioned boundary and illumination (recording) coverage conditions required to synthesize the boundary reflections are satisfied, at least for selected events, in both the seismic interferometry and virtual reflector data, and we focus our analysis to the comparison of the wavefields obtained with the representation theory. This is done with the main purpose to formulate and verify the combination theory (acoustic case) based on the Kirchhoff-Helmholtz integral representation.

SYNTHETIC EXAMPLES

We use synthetic examples to analyse the phase for the representation and combination of the virtual wavefields in 2D and 3D geometries, in which we assume complete coverage as an approximation. This is realized by a plane layer model, which is, in some way, equivalent to the case of a closed acoustic cavity (Poletto and Farina 2010a). The representation integrals are expressed by discrete trace-stacking equations, with the normal-incidence-ray approximation ($\cos\gamma = 1$), without the phase factors ($i\omega$) and ($-i\omega$) of equations (12) and (16). Taking into account the appropriate phase differences, this approximation of the Green's function does not entail the validity of the combination results. The analysis shows that the spatial-propagation operators take different forms in 2D and 3D.

2D acoustic model

We first analyse the combination of the virtual signals in 2D models. Synthetic seismograms are computed by a 2D finite-difference acoustic code. We simulate the signal propagation using two different models (Table 1) with the same source and receiver geometrical configurations. In the first application the entire model is a uniform background medium with acoustic velocity of 2000 m/s. In the second application the homogeneous background medium is bounded at the top and at the bottom by a strong-contrast medium (Fig. 3).

In both the unbounded and bounded models, two sources S_A and S_B are used in the background medium at the points A(2000, 2000) and B(2000, 900), respectively. The signals of the sources S_A and S_B are recorded by two horizontal lines of receivers positioned at a depth of 500 m (top line) and 3500 m (bottom line), respectively. These recording lines are located in correspondence of the boundaries of the contrast medium where we simulate the representation surface S_o. Here $S_o \equiv$ top line $\cup$ bottom line. In addition to the receivers on the

Table 1 2D acoustic model parameters

Horizontal dimension X	4000 m
Vertical dimension Z	4000 m
Pixel dimension $\Delta x = \Delta z$	2 m
Source (zero-phase) wavelet	Ricker
Source peak frequency	40 Hz
Output sampling time	1 ms
Propagation time	4 s

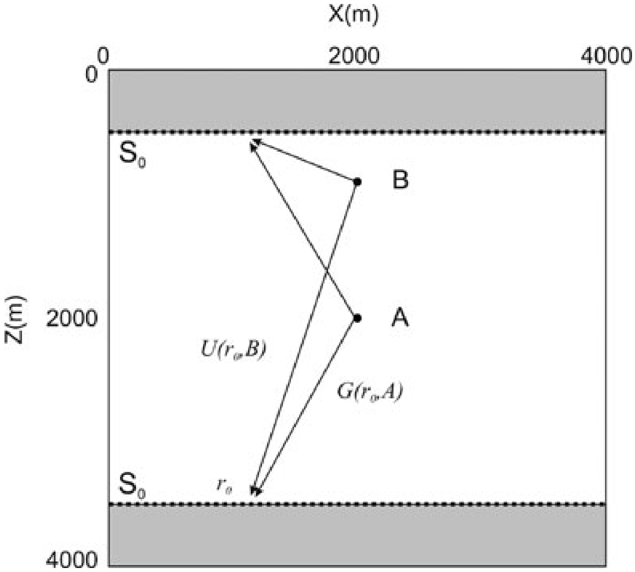

Figure 3 Acoustic model. The first horizontal layer (grey zone) represents the top contrast medium from 0–500 m depth. The second horizontal layer is the background medium from 500–3500 m depth. The third horizontal layer is the bottom contrast medium, from 3500–4000 m depth. The background medium velocity is 2000 m/s. The strong-contrast medium (grey zone) velocity is 20 000 m/s. Two sources are used in A(2000,2000) and B(2000,900). Receiver lines (dots) are located on S_o at the top and bottom reflecting interfaces.

representation surface S_o, the signals of the two sources are recorded by a vertical line of receivers passing in A and B for the control of the Green's function between the source points A and B.

Figure 4 shows the synthetic shots from the sources in A and B and recorded by the top and bottom line in the model with the contrast medium. These data are used for the combination of the interferometry by cross-correlation and virtual reflector signals. Figure 5 shows the traces of the vertical control receiver line passing in A and B with the source in B in the model with the contrast medium.

Before analysing the combination to separate the reflections in the model with the contrast medium, we analyse the direct wavefields in the background uniform model to evidence the basic differences in the propagated and composed wavefields. Figure 6 shows the input source (a zero-phase Ricker wavelet), the signal recorded at the source point B, i.e., the wavefield at the source sampled in space with the approximation of the grid spacing, and the signal propagated from B and recorded at the point A in the uniform model without boundary. This example shows that the wavelets in the 2D direct-modelled and propagated fields from the zero-phase source are non-zero phase ones. The signals are displayed in different time windows for comparison purposes. In the following examples the data of the uniform model are used for cross-convolution and cross-correlation, by composing the traces recorded at the top line. To obtain the cross-correlation trace, the signal from the source at A is cross-convolved with the time-reversal of the signal from the source at B. Figure 7 shows the individual (i.e., before surface-representation stacking) cross-correlation and cross-convolution signals for the central trace (at 2000 m) of the top recording line. The signals are displayed in different time windows for comparison purposes. We observe some important differences in the waveforms of the cross-composed traces a) and c), with phase-rotation effects that are discussed in more detail in the next section on result interpretation.

2D signal analysis and combination

In general, the virtual reflector method and interferometry may have different stationary-phase regions (Poletto and Farina 2008, 2010a). In this example they present the same stationary region at the central position (2000 m) of the top line. Figure 8 shows the cross-convolution and cross-correlation gathers of the top line (uniform model without boundary), which are displayed before stacking for stationary-phase analysis. The virtual reflector and interferometry obey different, elliptic and hyperbolic, stationary phase conditions (Poletto and Farina 2010a), arising in the surface integration of the terms $U(r_o, A)U(r_o, B)$ and $U(r_o, A)U^*(r_o, B)$. We may observe that this difference corresponds to upward convexity and concavity, respectively, in the signals of the stationary-phase gathers of Fig. 8.

In Fig. 9 we show the cross-composed signals of the uniform (no contrast medium) model before (trace at central-line position 2000 m) and after stacking of the cross-composed traces obtained on the representation surface (top recording line). Some differences in the waveforms obtained by 2D-wavefield propagation and representation integrals are discussed in the next section.

We use the model with top and bottom boundaries to obtain the virtual reflections also in the interferometry signals. Figure 10 shows the stationary travelpaths in the model with boundaries. The virtual signal estimation and the subtraction result are shown for selected events in Fig. 11, where we see (a) the interferometry signal containing the direct arrival between B and A and the top-layer reflection, (b) the virtual reflector signal from the top layer, and (c) the subtraction result. Some

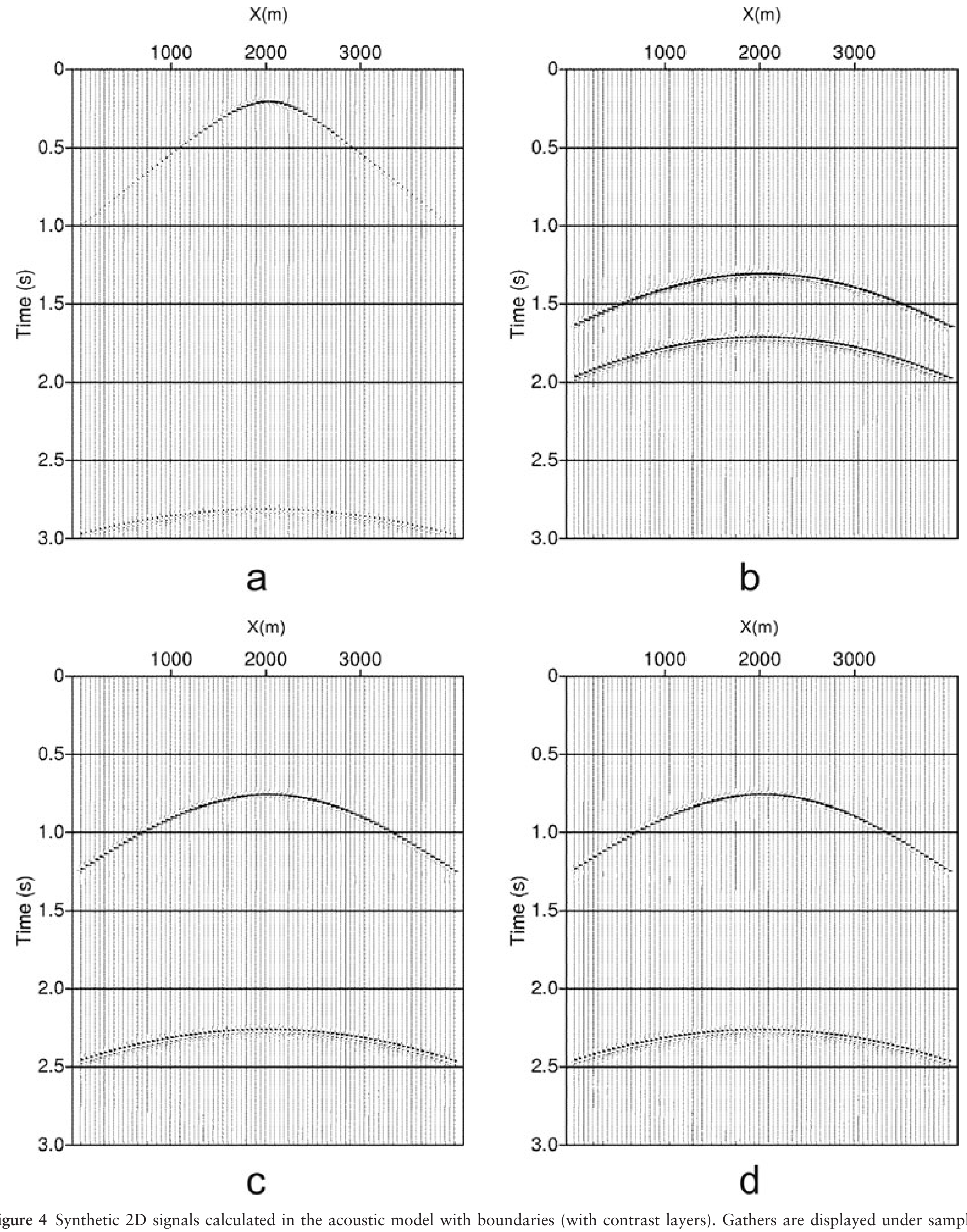

Figure 4 Synthetic 2D signals calculated in the acoustic model with boundaries (with contrast layers). Gathers are displayed under sampled with one trace every 25 traces for representation purposes. (a) Signals of the source in B recorded by the top line. (b) Signals of the source in B recorded by the bottom line. (c) Signals of the source in A recorded by the top line. (d) Signals of the source in A recorded by the bottom line.

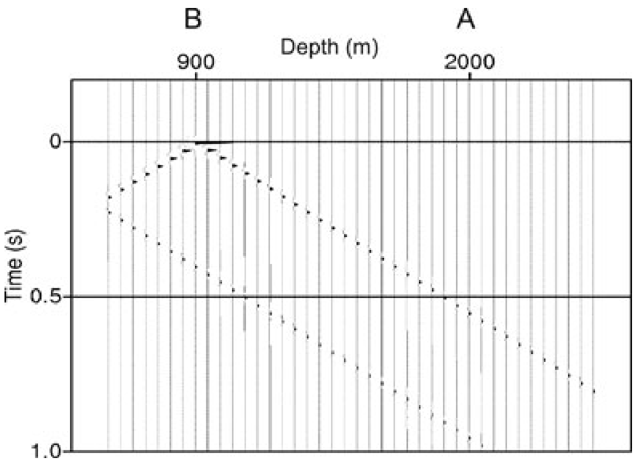

Figure 5 Synthetic 2D signals calculated in the acoustic model with boundaries (with contrast layers). The control receivers line passing in the source points A (depth 2000 m) and B (depth 900 m). The source is in B.

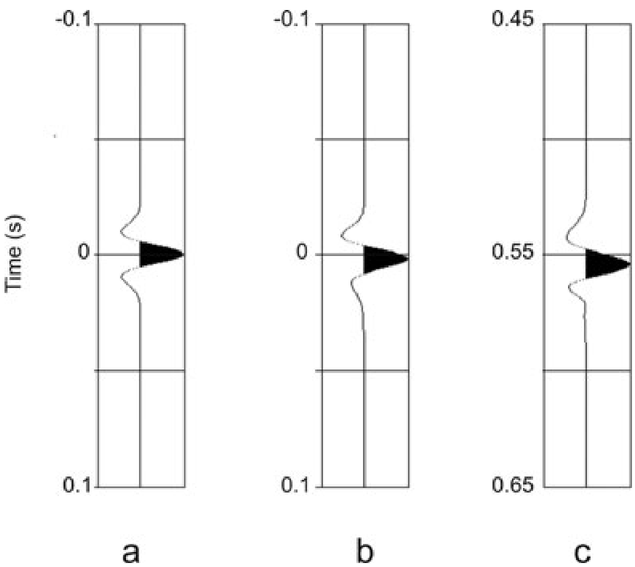

Figure 6 a) Zero phase Ricker source wavelet and control receiver signals calculated in the 2D acoustic model without boundaries (no contrast layers) and recorded (b) at the source point B and (c) at the point A.

lateral-trace tapering was applied to mitigate artefacts due to lateral-model dimensions.

3D acoustic model

Synthetic seismograms are computed by a 3D pseudospectral acoustic code (Carcione 2007), using a geometry similar to that of the 2D example. However, in the 3D case, the model dimensions and the source-signal central frequency were modified to optimize the calculation times and take into account model-size constraints, taking into account the aliasing condition in the larger 3D grid and the stationary conditions for the representation of seismic interferometry and virtual reflector signals, which may also be affected by artefacts due to lateral border effects.

We simulate the signal propagation using two different models (Table 2 and Table 3) with the same source geometrical configuration. In the first application the entire model is a uniform background medium of acoustic velocity 2000 m/s. In the second application the homogeneous background medium is bounded at the top and at the bottom by a strong-contrast medium.

In this last case the first horizontal layer represents the top contrast medium from 0–500 m depth. The second horizontal layer is the background medium from 500–3500 m depth. The third horizontal layer is the bottom contrast medium, from 3500–3960 m depth. The acoustic velocity of the strong-contrast medium is 20 000 m/s. In the uniform model two sources S_A and S_B are used in the background medium at the points $A = (990, 990, 2000)$ and $B = (990, 990, 900)$, respectively. In the non-uniform model (with a contrast medium) the sources S_A and S_B are used in the background medium at the points $A = (1800, 1800, 2000)$ and $B = (1800, 1800, 900)$, respectively. The difference in the dimensions of these models is due to the need to reduce side-border effects in the synthesis of the virtual reflections obtained by (SI) crosscorrelation, which have less moveout variations than the corresponding virtual reflector signals in the stationary gathers before stacking.

The uniform 3D model was used only to analyse the waveforms in the direct arrivals. As in the 2D case, the signals of the sources S_A and S_B are recorded by two horizontal planes of receivers positioned at a depth of 500 m (top plane for both the models), 2500 m (bottom plane for the uniform background model) and 3500 m (bottom plane for the model with a contrast medium). The recording planes at 500 m and 3500 m are located in correspondence of the boundaries of the contrast medium where we simulate the representation surface S_o. Also here $S_o \equiv$ top plane $\cup$ bottom plane.

Figure 12 shows the stationary signal analysis for a vertical section of the 3D datasets obtained by cross-convolution and cross-correlation in the uniform (no boundary) 3D model. We may observe that both the cross-convolution and cross-correlation wavelets before stacking are a close approximation of a zero phase signal (for comparison, see Figs. 8 and 9 where the

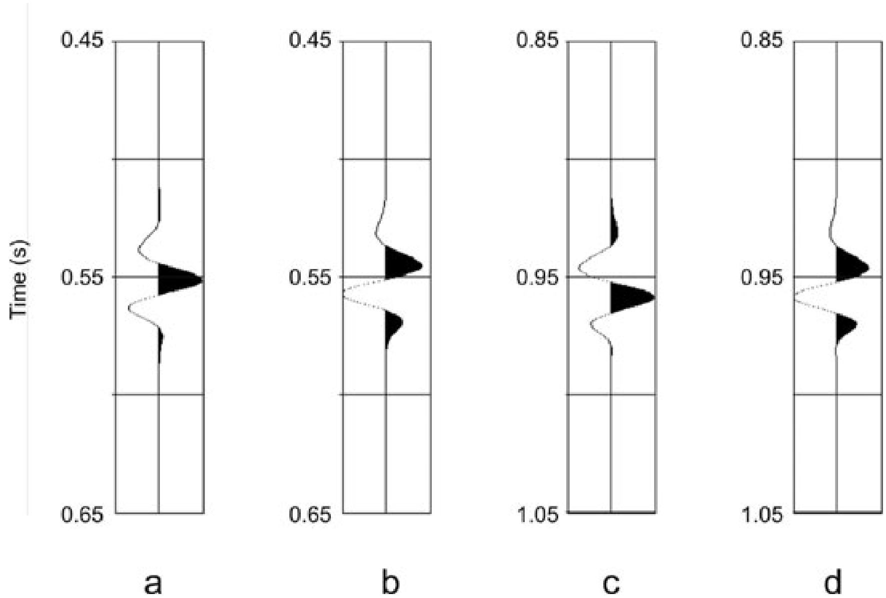

Figure 7 Signals calculated in the 2D acoustic model without boundaries (no contrast layers). a) Cross-correlated and c) cross-convolved traces (at central position 2000 m). b) Hilbert transform of the cross-correlated trace. d) Negative polarity cross-convolved trace.

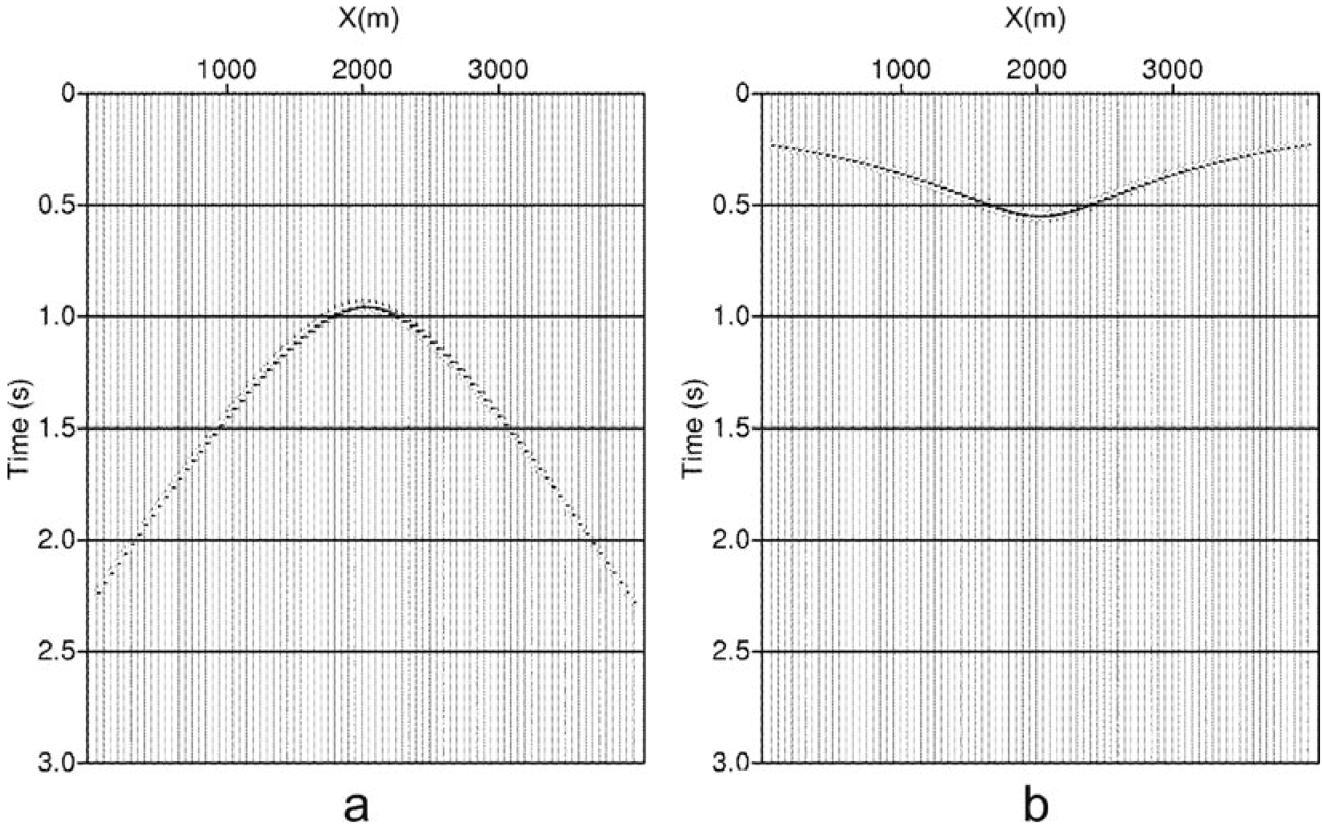

Figure 8 Signals calculated in the 2D acoustic model without boundaries (no contrast layers). Stationary phase analysis before stacking for a) virtual-reflector cross-convolutions and b) interferometry cross-correlations. These data are sampled every $\Delta x = 2$ m. In these figures the traces are represented every 50 m. Upward convexity (VR) and concavity (SI) cause different phases in the signals of the stacked traces.

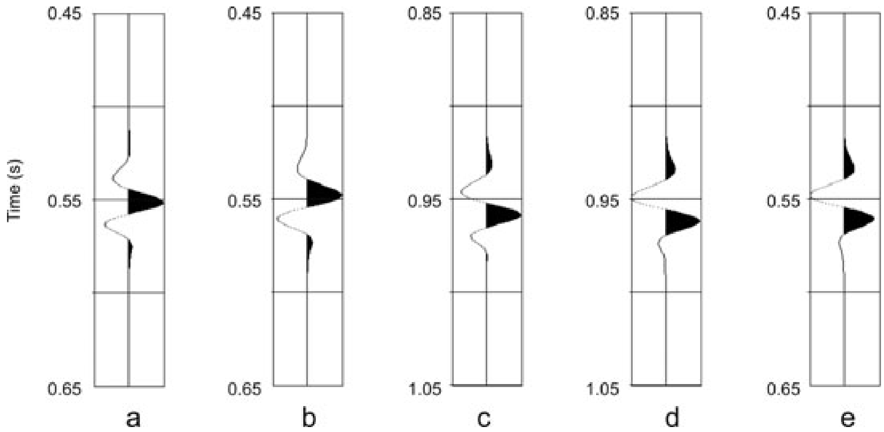

Figure 9 Signals calculated in the 2D acoustic model without boundaries (no contrast layers). Cross-correlated traces a) before (central position) and b) after line stack. Cross-convolved traces c) before (central position) and d) after line stack. e) Negative polarity cross-correlated stacked trace.

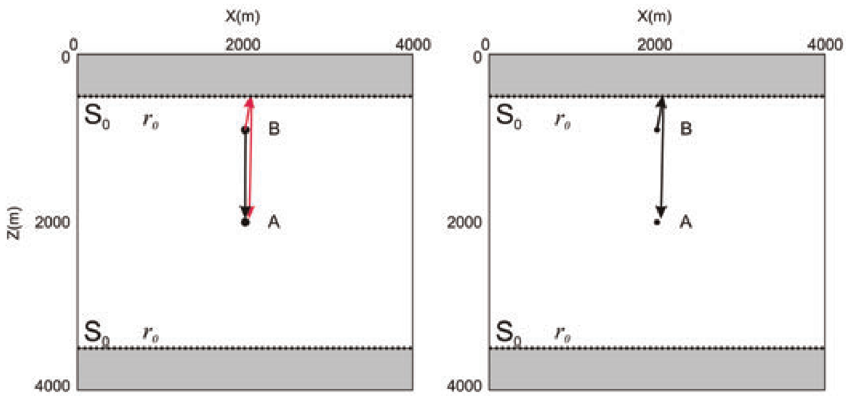

Figure 10 Stationary travelpaths of interferometry (left side) and virtual reflector (right side) in the 2D model with a contrast medium.

cross-correlation and cross-convolution wavelets before stack are different). With 3D data we can use different approaches to perform the stacking of the data recorded in the horizontal-plane dimensions (Fig. 13). The traces obtained by stacking the cross-convolved and cross-correlated traces of the 3D data set are shown with opposite polarity in Fig. 14. The reason of the opposite polarity, as for the 2D case, is discussed in the next section. Here, the virtual wavelets represent the direct seismic interferometry and the virtual reflector signals. These signals are contained in different time windows, and are aligned in the figure for representation purposes only.

Finally, Fig. 15 shows the results of the virtual-signal combination for selected events in the 3D model with boundaries similar to the 2D result of Fig. 11. These results are obtained using a surface representation integral. Figure 15 shows, from left to right, the interferometry signal, containing direct and top-boundary reflections, the virtual signal and the combination result. Some non-physical event due to lateral 3D model artefacts was removed by muting (instead of tapering).

RESULTS INTERPRETATION

We explain as follows the discrepancies in the representations of the acoustic wavefields in the 2D and 3D models. We underline the following main aspects.

Interpretation of the phase of the 2D results

In the theory the source signal is assumed to be zero phase (equation (1)). This is true for the injected input Ricker wavelet of the 2D synthetic example (Fig. 6a). However the control wavelet recorded at source position (b) has a different phase (also the signal in (c)). Moreover, in the cross-correlations and cross-convolutions before stack (equivalent to surface integration) of Fig. 7 we observe that the

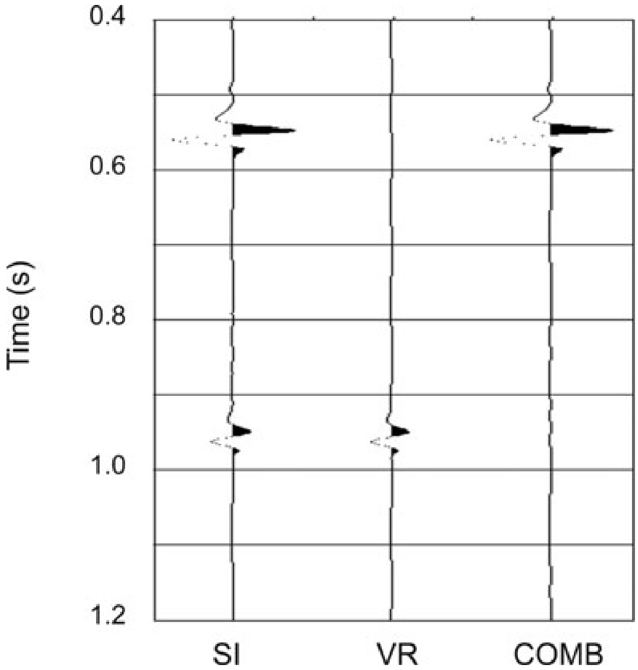

Figure 11 The traces represent a time window of the 2D virtual signals (selected events) in the model with boundaries. From left to right we have: SI, VR and combination, after scaling the virtual reflector signal by the reflection coefficient R = 0.8182. The first event is the direct arrival from B to A. The second event is the virtual signal from B to the top boundary and then reflected to A. The reflection event is subtracted in the last trace, a result of the combination.

Table 2 3D (uniform) model parameters

Horizontal dimension X	1980 m
Horizontal dimension Y	1980 m
Vertical dimension Z	3060 m
Pixel dimension $\Delta x = \Delta y = \Delta z$	10 m
Source (zero-phase) wavelet	Ricker
Source peak frequency	30 Hz
Output sampling time	1 ms
Propagation time	3 s

cross-correlation trace (a) and the cross-convolution trace (c) are different. Trace (b) is the Hilbert transform of the cross-correlation signal. It is nearly equal to the negative polarity cross-convolution trace (d). We interpret the 2D results as follows. We use a zero-phase monopole source in the 2D acoustic model, which is equivalent to a line source. The far-field Green's causal function of this source can be expressed in the Fourier frequency domain as

$$G^{(2D)}(r,\omega) = \frac{\exp\left[-i(\omega r/c + \frac{\pi}{4})\right]}{\sqrt{8\pi\omega r/c}}, \tag{19}$$

Table 3 3D (bounded) model parameters

Horizontal dimension X	3600 m
Horizontal dimension Y	3600 m
Vertical dimension Z	3960 m
Pixel dimension $\Delta x = \Delta y = \Delta z$	10 m
Source (zero-phase) wavelet	Ricker
Source peak frequency	30 Hz
Output sampling time	1 ms
Propagation time	3 s

where r is the radial distance from the source. Hence, the propagated signal signature recorded at the 2D receiver lines on S_o contains a $-\pi/4$ phase. This phase rotation disappears in the cross-correlation. It becomes $-\pi/2$ in the cross-convolution.

The next step is stacking over the (top) receiver line. We observe that (as expected) this causes another change in the signal phase (Fig. 9). We interpret this as follows: the integration in 2D produces a change in the phase of $\pi/4$ for cross-correlation, but results in $-\pi/4$ for cross-convolution. This is in agreement with the observation of stationary-phase convexity and concavity in Fig. 8 (the different distortion effect can be easily observed by integrating a trial zero-phase wavelet). This causes another $\pi/2$ relative difference in the stacked signals. Therefore the total phase difference is π, i.e., opposite polarity. This is what we observe if we compare Fig. 9(d) and 9(e).

Interpretation of the phase of the 3D results

We interpret the 3D results as follows. We use a zero-phase monopole source in the 3D acoustic model, which is equivalent to a point source. The Green's causal function of this source can be expressed in the Fourier frequency domain as

$$G^{(3D)}(r,\omega) = \frac{\exp\left[-i(\omega r/c)\right]}{4\pi r}. \tag{20}$$

This means that there is no phase distortion introduced in the signals recorded at the 3D receiver lines on S_o. Hence the cross-convolutions and cross-correlations contain zero-phase signals, as a good approximation (Fig. 12).

The next step is stacking over the (top) receiver line. We observe that (as expected) this causes another change in the signal phase (Fig. 14). We interpret this as follows: the integration in 3D produces a change in the phase of $-\pi/2$ for cross-correlation, but results in $\pi/2$ for cross-convolution, due to the different convexity properties of the stationary curves (Fig. 12). Also in this case, as in 2D but for different reasons, this causes a total relative phase rotation of π in the

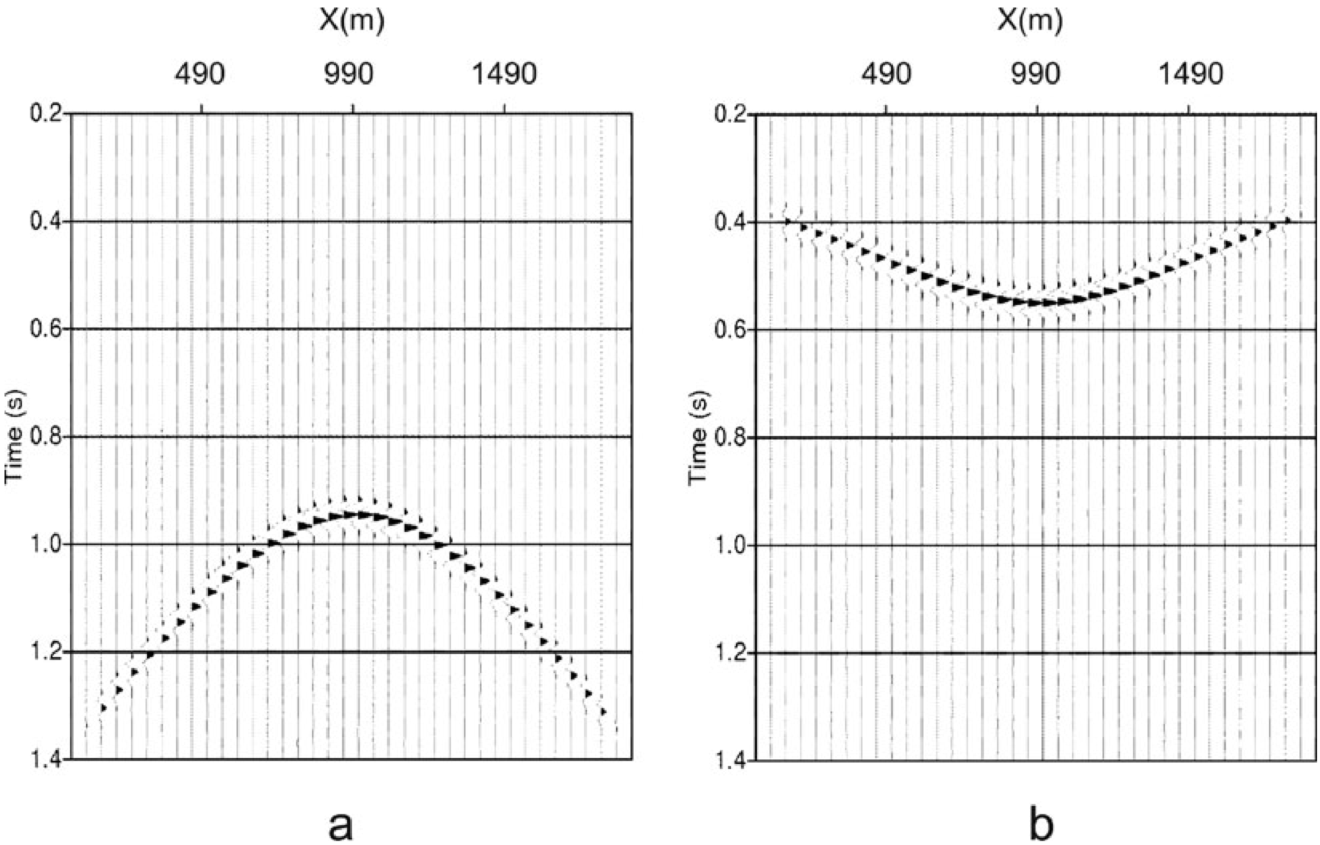

Figure 12 Signals calculated in the 3D acoustic model without boundaries (no contrast layers). Stationary phase analysis for a) virtual-reflector cross-convolutions and b) interferometry cross-correlations. These data are sampled with a larger space interval ($\Delta x = 10$ m) with respect to the corresponding 2D example of Fig. 8 (where $\Delta x = 2$ m) because of the computational cost. In the figure the traces are represented every 50 m to observe better the waveforms of the individual signals.

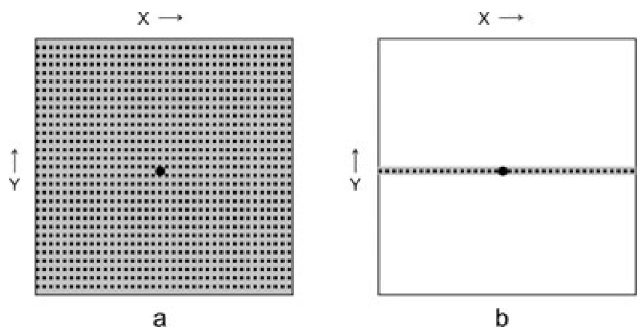

Figure 13 Top views of the 3D model with a) the surface and b) line integrals, which give different phase contributions in the synthesis of the virtual signals.

signals given by the simple correlation/convolution and stacking algorithms and the result is opposite polarity between corresponding events in the cross-correlated and cross-convolved signals, as in Fig. 14 where we compare direct and top-boundary reflection for waveform analysis.

SUMMARY AND DISCUSSION

We calculate and analyse different phases of the virtual reflector and seismic interferometry signals in 2D and 3D. Note that the factors $(i\omega)$ (in equation (12)) and $(-i\omega)$ (in equation (16)) are necessary to end up with the correct phase of the retrieved Green's function. For example: in the 2D cross-correlation the integral causes a $\pi/4$ phase shift. Then the factor $(-i\omega)$ causes $-\pi/2$. Together this gives $-\pi/4$, which is indeed the correct phase of the 2D retrieved Green's function. Again, in the 3D cross-correlation the surface integral causes $\pi/2$. Then the factor $(-i\omega)$ causes $-\pi/2$. Together this gives 0, which is indeed the correct phase of the 3D retrieved Green's function.

We summarize below the phase differences for the combination purposes with the virtual reflector and seismic interferometry stacking equations $(\Sigma_k G_k U_k)$ and $(\Sigma_k G_k U_k^*)$, with index k over the same domain of sources or, reciprocally, receivers.

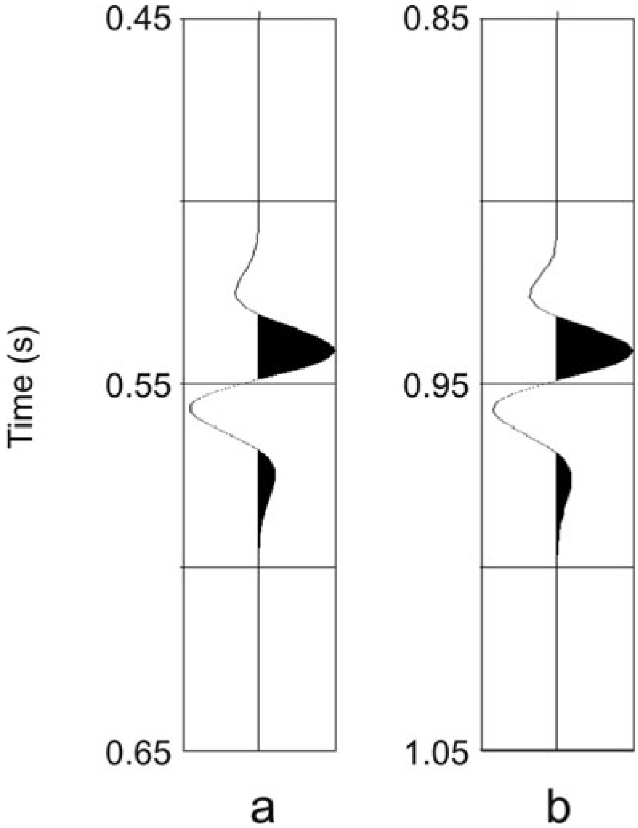

Figure 14 (a) Interferometry direct signal and (b) virtual reflector (VR) signal (opposite polarity) obtained by surface integration in the 3D acoustic model without boundaries, and shown for signal-waveform analysis purposes.

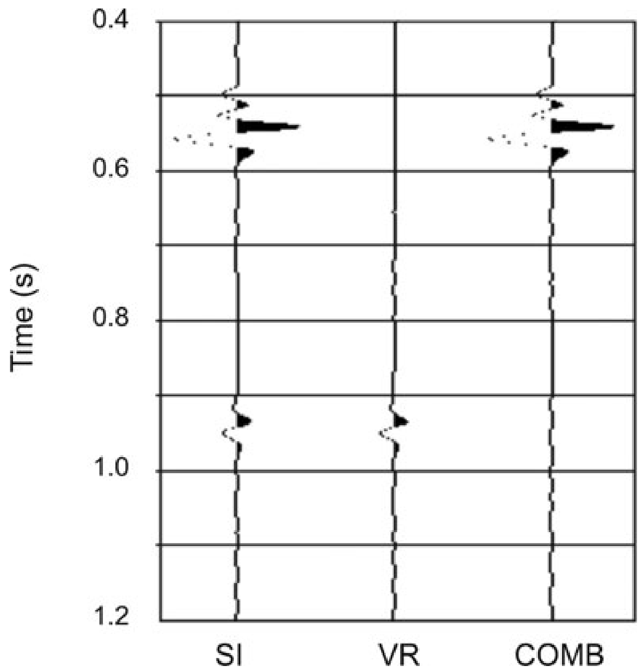

Figure 15 The traces represent a time window of the 3D virtual signals (selected events) obtained by surface integral in the model with boundaries. From left to right we have: SI, VR, and combination, after scaling the virtual reflector signal by the reflection coefficient R = 0.8182. The first event is the direct arrival from B to A. The second event is the virtual signal from B to the top boundary and then reflected to A. The reflection event is subtracted in the last trace, a result of the combination.

- In 2D acoustic data (synthetic by line source) we obtain seismic interferometry and virtual reflector waveforms with opposite (π phase) polarity. This is due to two composite effects: the phase difference is due to the opposite ($\pi/4$) and ($-\pi/4$) phases of the integrals; another $-\pi/2$ phase difference is due to the $-\pi/4$ phase of the far-field Green's function from a line source, thus giving 0 for correlation and $-\pi/2$ for convolution. The total phase difference is $\pi = \pi/4 - (-\pi/4 - \pi/2)$.
- In 3D acoustic data, by a surface representation integral, the signature of the Green's function from a point source is zero-phase. An opposite sign comes in the virtual signals from the differential phase shift $\pi = \pi/2 - (-\pi/2)$ introduced by the surface-representation integrals.
- In 3D acoustic data, by a line representation integral, the signature of the Green's function from a point source is zero-phase. A $\pi/2$ phase (Hilbert transform) comes from the differential phase shift $\pi/2 = \pi/4 - (-\pi/4)$ introduced by the line-representation integrals. Figure 16 shows the 3D result obtained using a line integral for representation and Hilbert transforming the virtual reflector data before combination (compare with Fig. 15).

EXAMPLE OF SEISMIC SIGNAL COMBINATION IN A 3D OCEAN BOTTOM SEISMIC MODEL

Advantages and possible applications of the virtual-reflector and seismic-interferometry combination method are illustrated and discussed for example in Poletto and Farina (2010b). Here we use a similar ocean bottom seismic (OBS) marine application and analyse the combination of virtual signals in a 3D acoustic model by using multiple energy to illuminate the interferometry signals from the sea bottom.

Synthetic seismograms are computed by a 3D pseudospectral acoustic code. The model (Table 4) is made up of horizontal layers, with a water layer 600 m thick with an acoustic velocity c_p = 1500 m/s, which lies on a 800 m formation layer with c_p = 2800 m/s, which, in turn, lies on a

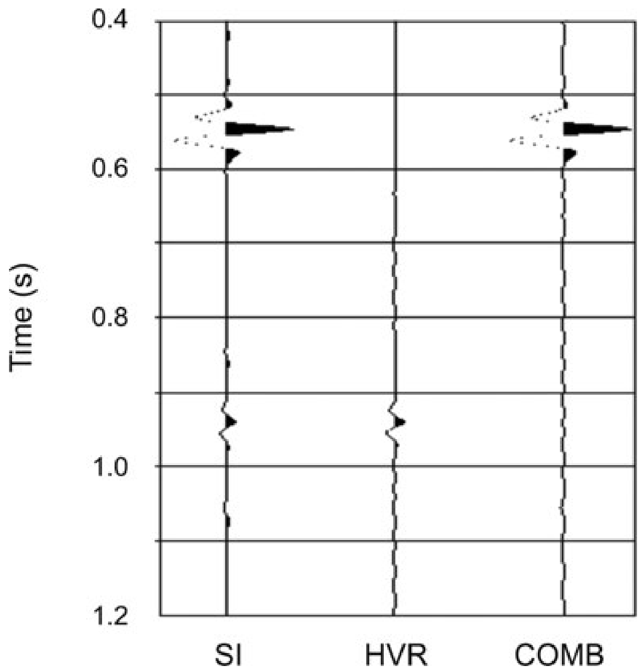

Figure 16 The traces represent a time window of the 3D virtual signals (selected events) obtained by a line integral in the model with boundaries. We may observe a difference in the amplitude of the reflected signal with respect to Fig. 15, interpreted as a non complete reconstruction for propagation effects when using the 2D integral in 3D. From left to right we have: seismic interferometry (SI), virtual reflector (VR) and combination, after Hilbert transforming and scaling the virtual reflector signal. The first event is the direct arrival from B to A. The second event is the virtual signal from B to the top boundary and then reflected to A. The reflection event is subtracted in the last trace, a result of the combination.

Table 4 3D OBS model parameters

Horizontal dimension X	3900 m
Horizontal dimension Y	3900 m
Vertical dimension Z	2040 m
Pixel dimension $\Delta x = \Delta y = \Delta z$	10 m
Source (zero-phase) wavelet	Ricker
Source peak frequency	30 Hz
Output sampling time	1 ms
Propagation time	4 s

440 m formation layer with $c_p = 4800$ m/s. The water layer is bounded at the top by 200 m of vacuum (simulated by a very low velocity medium).

A pressure source is used at the centre of the model in the first pixel of the water layer at the point S = (1950, 1950, 210). To save computational costs (in terms of computing time and memory), we calculated the shots that are input for

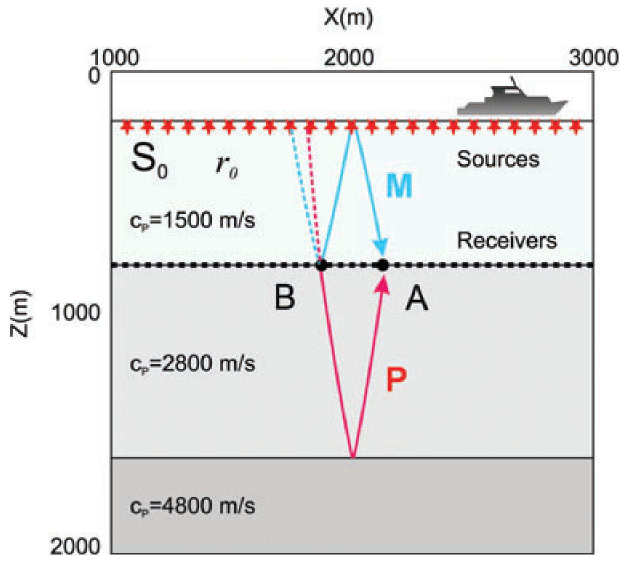

Figure 17 Marine model used for 3D representation and signal combination. The arrows show the stationary seismic interferometry and virtual reflector raypaths. M indicates the water-layer reflection and P denotes a primary reflection.

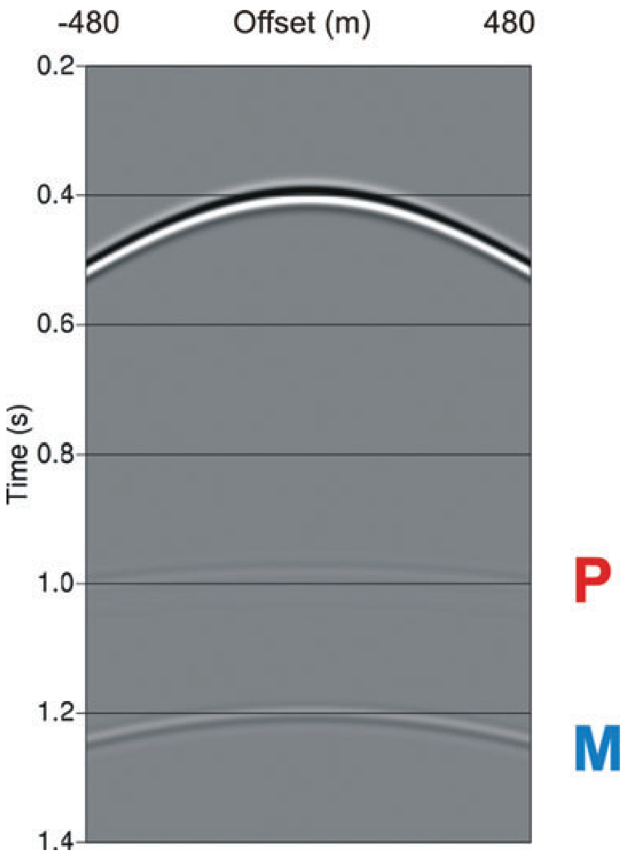

Figure 18 Marine synthetic data used for 3D representation. Example of direct modeled data, 2D section from a 3D dataset. P indicates a primary reflection and M a water layer multiple.

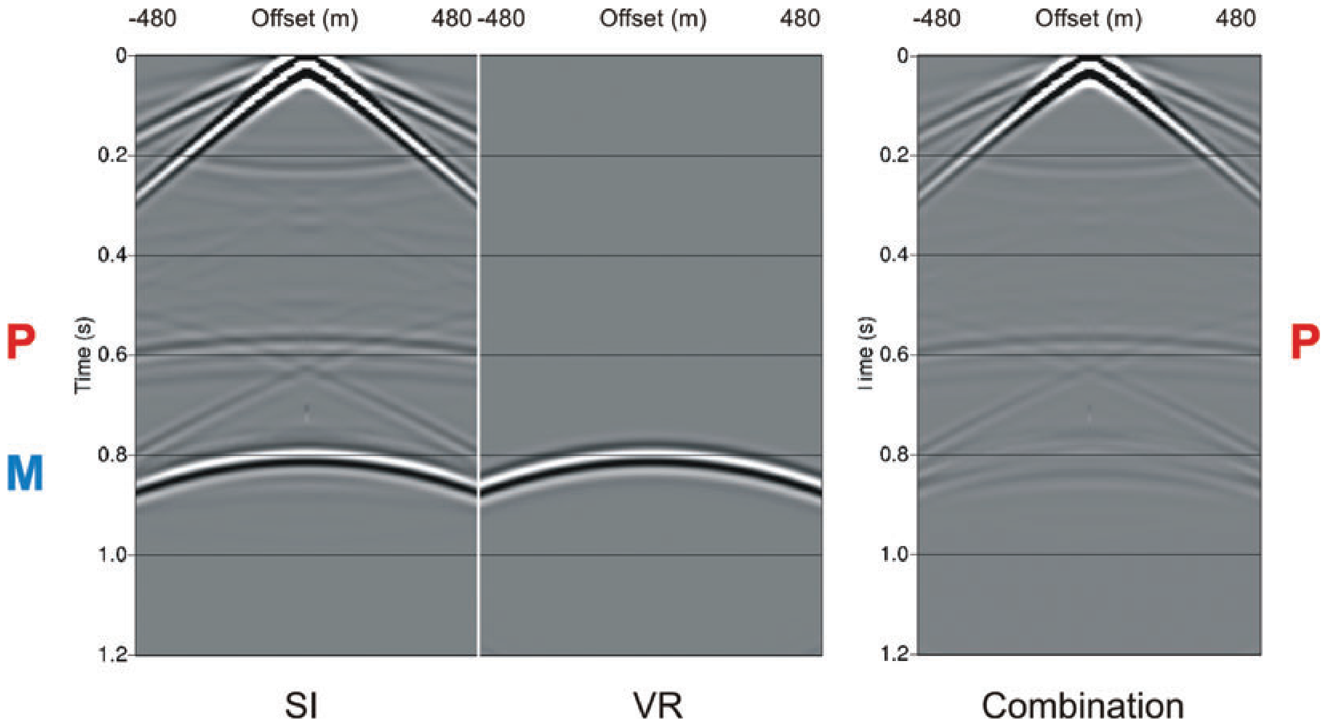

Figure 19 Virtual signals of the 3D marine model with line-integral representation. The virtual reflector data are Hilbert transformed, scaled and compared to the seismic interferometry data. The panel on the right side shows the result of the combination, where the multiple M is removed.

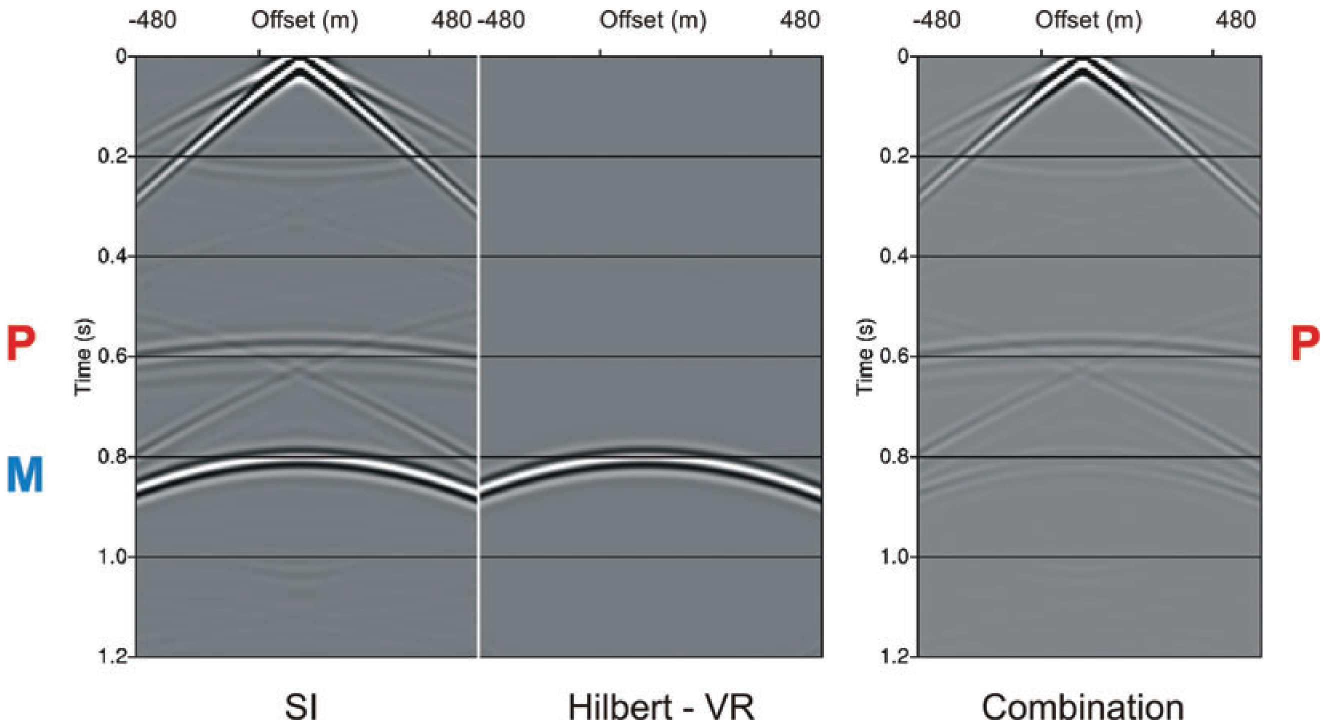

Figure 20 Virtual signals of the 3D marine model with surface-integral representation. The virtual reflector data are scaled and compared to the seismic interferometry data. The panel on the right side shows the result of the combination, where the multiple M is removed.

interferometry and the virtual reflector method by extracting and reorganizing the trace gathers obtained with a single numerical simulation in the horizontally layered model. With this approach, we simulate a two-dimensional array of sources located at different positions at the water surface in models with smaller lateral dimensions (with side dimensions approximately half the original ones).

The signals are recorded by receivers located at the seabottom, to simulate an ocean bottom seismic dataset. Figure 17 shows a side view of the marine model, with stationary travelpaths for interferometry and virtual reflector wavefields. Figure 18 shows an example of a 2D cross-section of the shot in the 3D model.

The virtual signals are both calculated by integrating (stacking) in the domain of the sources, at the representation surface *S*, the cross-correlations and cross-convolutions of the signals of couples of receivers. This application is similar to the 2D example of water-layer multiples removal by a virtual wavefield combination of selected events shown by Poletto and Farina (2010b) (they discussed the approaches based on a selection of events before and after virtual reflector convolution) and it is analysed here for wavefield representation purposes in a 3D acoustic model.

Figure 19 shows the result of the 3D signal combination in selected time windows, with the line-representation integral. In this case we apply a Hilbert transform before subtracting the virtual reflector signals. The agreement of the multiple reflection (M) in the seismic interferometry and virtual reflector signals is good and after combination the primary reflection (P) is preserved with an improved S/N.

Figure 20 shows the full-3D application similar to that of Fig. 19 but using the surface-integral representation. In these examples, some noise is present in the form of interferometry artefacts, side-border modelling and end-point truncation effects. These effects are more important because of the limited dimensions of the 3D model for very high computational costs. We attenuated in part this noise by tapering the input signals to smooth the truncation effects and by windowing the virtual signals to mitigate the interferometry spurious events. However, some residual noise is still present in the final results. Also in this case the subtraction of the water-layer multiple (M) in the right panel is good, especially at short offsets where the coverage conditions for the reconstruction of the virtual signals are more complete. The primary reflection (P) is preserved with improved S/N. In this case we apply the opposite-phase rotation taking also into account the changes of phase introduced by the surface-source ghost and the free-surface reflection coefficient.

CONCLUSIONS

We present the 2D and 3D phase analysis for the integral representation and combination of virtual signals in an arbitrary, inhomogeneous acoustic medium. The analysis of the virtual boundary reflections shows that, beyond a reflection coefficient operator, the combination coefficients of the representation integrals depend on initial source waveform, and propagation Green's function distortions. Different results are obtained for virtual data representation and subtraction in 2D and 3D. An opposite-sign coefficient is calculated both for combination of 2D and 3D data, but for different reasons. The phase of the virtual signals is analysed in examples of subtraction of common boundary reflections in redatumed virtual signals with complete coverage conditions. The method can be used with real seismic data propagated in 3D, with different phase shifts for line-integral and surface-integral representations, e.g., like with marine data.

REFERENCES

Bakulin A. and Calvert R. 2006. The virtual source method: Theory and case study. *Geophysics* **71**(4), SI103–SI110.

Carcione J. M. 2007. Wave fields in real media: Theory and numerical simulation of wave propagation in anisotropic, anelastic, porous and electromagnetic media. Second edition, *Handbook of geophysical exploration*, Seismic exploration, Elsevier Science, Amsterdam, The Netherlands.

Curtis A., Nicolson H., Halliday D., Trampert J. and Baptie B. 2009. Virtual seismometers in the subsurface of the Earth from seismic interferometry. *Nature Geoscience*, DOI: 10.1038/NGEO615.

Draganov D., Wapenaar K. and Thorbecke J. 2006. Seismic interferometry: Reconstructing the earth's reflection response. *Geophysics* **71**(4), SI61–SI70.

Halliday D. F., Curtis A., Vermeer P., Strobbia C., Glushchenko A., van Manen D.-J. and Robertsson J. O. A. 2010. Interferometric ground-roll removal: Attenuation of scattered surface waves in single-sensor data. *Geophysics* **75**, SA15–SA25.

Poletto F. and Farina B. 2008. Synthesis of a Virtual Reflector by processing recorded seismic signals. 70th EAGE Conference, Rome, Expanded abstracts, P271.

Poletto F. and Farina B. 2010a. Synthesis of a seismic virtual reflector. *Geophysical Prospecting* **58**(3), 375–387.

Poletto F. and Farina B. 2010b. Synthesis and composition of virtual-reflector (VR) signals. *Geophysics* **75**(4), SA45; doi: 10.1190/1.3433311.

Poletto F. and Wapenaar K. 2009. Virtual reflector representation theorem (acoustic medium). *Journal of the Acoustical Society of America* **125**(4), EL111–EL116.

Poletto F., Wapenaar K. and Bellezza C. 2010. Kirchhoff-Helmholtz Representation for Interferometry and Virtual Reflectors in Acoustic Media. 72nd EAGE Conference, Barcelona, Expanded abstracts, G014.

Schuster G. T. 2009. Seismic Interferometry. Cambridge University Press, UK.

Slob E. and Wapenaar K. 2007. Electromagnetic Greens functions retrieval by crosscorrelation and cross-convolution in media with losses. *Geophysical Research Letters* **34**, L05307.

Snieder R. 2004. Extracting the Green's function from the correlation of coda waves: A derivation based on stationary phase. Phys. Rev. E 69, 046610.

Wapenaar C. P. A. 1993. Kirchhoff-Helmholtz downward extrapolation in a layered medium with curved interfaces. *Geophys. J. Int.* **115**, 445–455.

Wapenaar K., Draganov D. and Robertsson J. 2008. Seismic interferometry: History and present status. *Society of Exploration Geophysicists*, Geophysics Reprint Series No. 26, ISBN 978-1-56080-150-4.

Wapenaar K. and Fokkema J. 2006. Greens function representation for seismic interferometry. *Geophysics* **71**(4), SI33–SI46.

Wiggins W. 1988. Attenuation of complex water-bottom multiples by wave-equation-based prediction and subtraction. *Geophysics* **53**, 1527–1539.

Wiggins W. 1999. Multiple attenuation by explicit wave extrapolation to an interpreted horizon. *The Leading Edge*, 46–54.